Jurnal Ilmu Komputer dan Informasi (Journal of Computer Science and Information)
17/2 (2022), 203-218. DOI: http://dx.doi.org/10.21609/jiki.v17i2.1298

Automated Ultrasound Object Segmentation Using Combinatorial Active Contour Method

Anan Nugroho[1*], Budi Sunarko[2], Hari Wibawanto[3], Anggraini Mulwinda[4], Anas Fauzi[5], Dwi Oktaviyanti[6], Dina Wulung Savitri[7]

Faculty of Engineering, Universitas Negeri Semarang, Gunungpati, Semarang, 50229, Indonesia

E-mail: [1*]*anannugroho@mail.unnes.ac.id,* [2]*budi.sunarko@mail.unnes.ac.id,*
[3]*hariwibawanto@mail.unnes.ac.id,* [4]*anggrainimulwinda@mail.unnes.ac.id,*
[5]*anasfauzi41@students.unnes.ac.id ,* [6]*dwioktaviyanti@students.unnes.ac.id,*
[7]*dina60108@students.unnes.ac.id*

Abstract

Active Contour (AC) is an algorithm widely used in segmentation for developing Computer-Aided Diagnosis (CAD) systems in ultrasound imaging. Existing AC models still retain an interactive nature. This is due to the large number of parameters and coefficients that require manual tuning to achieve stability. Which can result in human error and various issues caused by the inhomogeneity of ultrasound images, such as leakage, false areas, and local minima. In this study, an automatic object segmentation method was developed to assist radiologists in an efficient diagnosis process. The proposed method is called Automatic Combinatorial Active Contour (ACAC), which combines the simplification of the global region-based CV (Chan-Vese) model and improved-GAC (Geodesic Active Contour) for local segmentation. The results of testing with 50 datasets showed an accuracy value of 98.83%, precision of 95.26%, sensitivity of 86.58%, specificity of 99.63%, similarity of 90.58%, and IoU (Intersection over Union) of 82.87%. These quantitative performance metrics demonstrate that the ACAC method is suitable for implementation in a more efficient and accurate CAD system.

Keywords: *Active contour, automated, CAD, segmentation, US*

1. Introduction

Ultrasonography (US) is the most used medical imaging modality for screening glandular and tissue abnormalities due to its affordability, non-invasiveness, and ease of use. The ability of US to generate real-time and fast image results makes it highly efficient for large-scale and repeated examinations. Despite all its advantages, interpreting US images is subjective and highly dependent on the expertise, skills, and experience of the radiologist, leading to high variability in the diagnostic process [1]. The inadequate quality of US, such as poor resolution or low contrast, further complicates visual analysis and increases the potential of misinterpretation [2].

To address these challenges, Computer-Aided Diagnosis (CAD) technology has rapidly developed by implementing various image-processing algorithms and pattern-recognition techniques [3]. CAD aims to provide objective information to radiologists as a second opinion to support diagnosis. The procedural process in CAD systems typically involves image acquisition, preprocessing, segmentation, feature extraction, classification, and obtaining accurate diagnostic results [4].

Segmentation plays a crucial role in CAD systems by accurately separating lesions and nodules from the surrounding tissue [5]. The segmentation stage encounters challenges arising from variations in image quality. US images exhibit characteristics such as non-uniform intensity texture distribution and blurred object edges, which complicate the segmentation process. These complications are primarily caused

by the influence of speckle noise and the presence of various artifacts in US images. Speckle noise is the main cause of blurred object appearance and indistinct boundaries [6]. On the other hand, artifacts refer to pixel defects resulting from manual addition of descriptive attributes by machines or operators, such as text, notations, lines, or symbols [7].

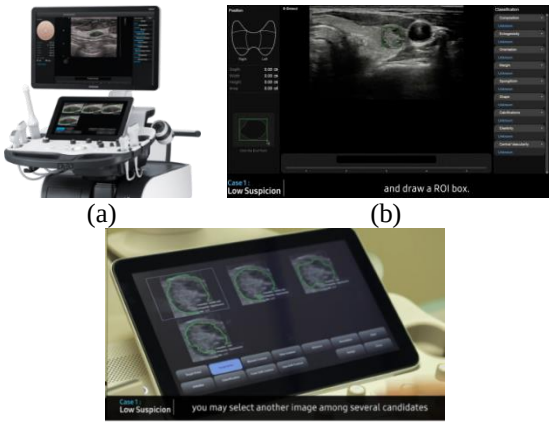

Figure 1. Ultrasound: S Detect for Thyroid RS80 (a) RS80 Machine, (b) Manual Segmentation, (c) Segmentation Results [8]

Computer-Aided Diagnosis (CAD) has been extensively developed for several ultrasound machines. One of them is Ultrasound: S Detect for Thyroid RS80 developed by Samsung Medical Imaging, as shown in Figure 1 point (a) [8]. The RS80 is not only used for detecting thyroid cancer but also breast lesions [9]. However, the machine still has weaknesses in the segmentation stage. In this stage, for segmentation to occur, radiologists still need to manually initialize the location of cancer objects, as seen in Figure 1 point (b), and choose the desired segmentation results, as shown in Figure 1 point (c). This process is not efficient and increases the chances of human error when repeated for a large number of patients. Yet, segmentation plays a crucial role in US imaging with CAD systems [10]. Segmentation in CAD systems is used to separate nodular or lesion areas from the surrounding tissue (background) [11]. The segmentation is crucial role as it is used to obtain objective data such as geometric information, shape, edge boundaries, and texture as part of the feature extraction process. Well-segmented lesion and nodule objects will provide accurate and objective diagnostic conclusions [12]. The selection of methods used in each stage of CAD needs to be carefully considered to achieve optimal results.

Among the existing methods, the active contour (AC) model variation is an efficient approach that can be developed into a specialized image segmentation technique [13]. Surveys from several studies [14]–[20] show that deformable AC models are the most widely applied approach in segmenting US images. The two of them are a review of segmentation methods in US breast by Xian et al. [17] and thyroid by Nugroho et al. [17] as reported in Figure 2.

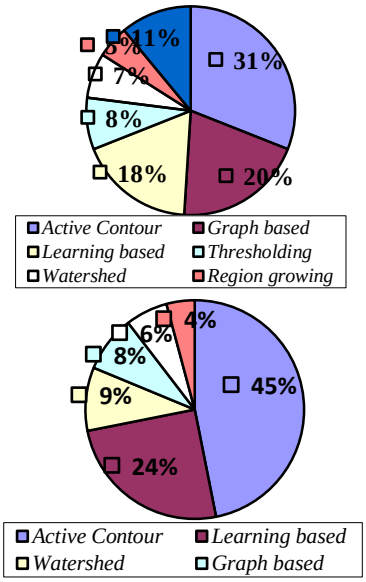

Figure 2. Distribution of breast (above) and thyroid (under) segmentation methods.

AC is a dynamic curve that evolves in the normal plane of image and stops at the gradient of edge or at the border of intensity change. An AC simulation on synthetic images segmentation is shown in Figure 3. The first line of Figure 3 (a,b) shows that AC is able to provide accuracy of segmentation in the object topology with the dominance of sharp curves. The second line of Figure 3 (c,d) illustrates that AC evolution is able to segment multiple objects simultaneously. Dynamic object topologies are also able to be handled effectively by AC. The flexibility of closed-curves AC is capable to accurately separate object boundaries in various biological network tissues and allows users to integrate with other frameworks if needed to improve performance. This cannot be done by conventional segmentation methods such as edge detection, thresholding and classical morphological operations [21].

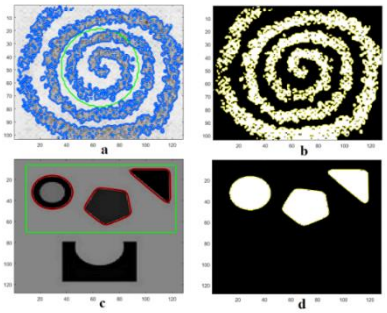

Figure 3. AC segmentation on the rough (a,b) and multiple (c,d) objects.

Well-established interactive approaches such as region growing and graph cut are also not appropriate for large-scale segmentation as they are inefficient [20]. Whereas the most prominent weakness of all learning-based approaches is that they are highly dependent on training data. If there is not a higher amount of dataset available, it is less possible to get a significant performance increase [20]. Moreover, radiological US objects are specific so global segmentation approaches such as watershed and clustering based methods tend to produce inaccurate results. While AC can segment specific objects without requiring a long preprocessing stage. With this capability, AC is very robust for a wide variety of applications. This method is built based on a mathematical model involving parameters and variables that are adjustable so it has the opportunity to be generated as an automatic segmentation technique.

Existing AC models still retain an interactive nature. This is due to the large number of parameters and coefficients that require manual tuning to achieve stability. A stable AC model is characterized by convergent trends in the change in length and area of the curve during evolution. Convergence is the ability of an AC model to stop exactly at the expected object segmentation. The more converging, the AC model will be more reliable and resilient. Despite this, a high number of parameters or coefficients in an AC model can lead to increased operator intervention, making it impractical. The segmentation process becomes complicated and difficult.

In addition, US inhomogeneity negatively effects the evolution so that the curve is trapped in the false area (FA) or false regions that are not the real object segmentation as shown in Figure 4 point (a). FA includes two possibilities, which are non-lesion areas that are segmented as lesions (false positive-FP) and areas of lesions that are segmented as non-lesion areas (false negative-FN). Inhomogeneity also results in leakage problems in the evolution of curve AC. Leakage is a term for the evolution of curves that penetrate or hit object boundaries because of weak edge gradients or the blurring of intensity between objects and their backgrounds. Leakage is shown in Figure 4 (b). In the severe noisy conditions, even the AC curve cannot move at all because it is trapped in the local minima (LM) area as illustrated in Figure 4 (c). LM is an area that can hardly be detected by the presence of a gradient around the edge so that it cannot be distinguished between objects and backgrounds. LM is the opposite condition to leakage in the phenomenon of AC evolution. Indeed, homogeneous images will be easier to segment with AC model. Thus, the adaptation of an AC model to be robust against noise and inhomogeneity is also a matter of great concern.

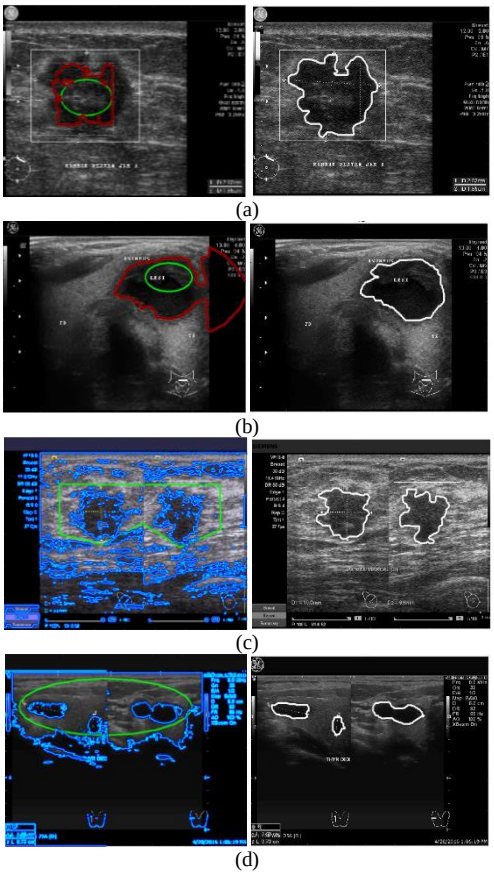

Figure 4. AC segmentation problems on ultrasound images locally (red contours) and globally (blue contours). (a) Local minima (LM), (b) Leakage, and (c-d),False area (FA), with their ground truth on right side.

Ground truth (GT) refers to the meticulous segmentation results performed by experts through a manual process by a number of radiologists who have reached a consensus. Thus, a valid GT reference is obtained without any variability concerns. In this study, GT was created by Dr. Lina Choridah, Sp. Rad., and her students

in the Department of Radiology, Faculty of Medicine, Universitas Gadjah Mada.

Combinatorial AC model will realize a practical and efficient CAD system. Automation is applied to reduce the dependence of AC on operator intervention. The development of the AC model by integrating this point is the biggest challenge in this work due to the diverse quality of US images.

1.1 Gaps Among Existing AC Models

In principle, all AC methods adopt three basic categories of AC models: parametric Snakes [22], edge-based geodesic active contour (GAC) with local edge information [23], and global region-based Chan-Vese (CV) [24]. Each method differs only in the application of preprocessing techniques and optimization methods. Besides these three categories of AC models, there are still many AC models that have not been used as methods for US image segmentation. One of them is the hybrid model category. The following explanation will provide an overview of the development of various AC models.

The concept of contour explicit parametric models, particularly in the realm of computer vision and image processing, has given rise to innovative techniques such as edge-based active contours (AC). One noteworthy example of these models is the Snakes model and its evolution into the ADF (Active Deformable Framework). These models leverage supporting algorithms like Balloon Force and GVF (Gradient Vector Flow) to enhance their effectiveness in capturing complex shapes and contours within images. A notable contribution of these approaches lies in their ability to address challenges related to concave structures and specific segmentation tasks. Recognizing their limitations is crucial, as these methods might lack flexibility and encounter challenges in scenarios involving merging and splitting. This underscores the continuous pursuit of advancements in contour parametric modeling for applications that are more robust and versatile. [6], [22], [25].

The concept of implicit geometric and variational level set methods has significantly contributed to the advancement of edge-based active contours (AC) in the field of image processing and computer vision. Within this category, the Geodesic Active Contour (GAC) model stands out as a fundamental representation of these techniques. Supporting algorithms such as DRLSE (Distance Regularized Level Set Evolution) and RDLSE (Region-based Distance Regularized Level Set Evolution) have played crucial roles in refining and optimizing the performance of these models. One notable contribution of these approaches is their efficacy in regularization, allowing for more stable and accurate contour evolution. Additionally, they exhibit a commendable degree of flexibility in handling complex scenarios involving the merging and splitting of contours. It's essential to acknowledge certain weaknesses, including the reliance on trial and error in the Explicit Shape Feedback (ESF) process, potential issues of leakage, and challenges associated with Level Set Methods (LM). Addressing these limitations remains an ongoing area of research to further enhance the applicability and robustness of implicit geometric and variational level set models in diverse image analysis tasks. Caselles et al. 1997; Li et al. 2010; Malladi et al. 1995; Osher and Sethian 1988; Zhang et al. 2013).

The concept of implicit geometric and variational level set methods has found application in the domain of global region-based active contours (AC), showcasing its versatility in image processing and computer vision. Various models, such as CV/ACWE (Chan-Vese/Active Contour Without Edges), RBSPF (Region-Based Shape Prior Fields), MLSAC (Multi-Level Set Active Contour), and ILF (Implicit Level Set Function), exemplify the diversity within this category. These models make significant contributions to the field by demonstrating robustness in handling initial contours, incorporating Explicit Shape Feedback (ESF), and effectively leveraging gradient information for contour evolution. Despite these strengths, a notable weakness arises when these models encounter challenges in the form of being trapped in false attractors (FA) in the presence of heterogeneous images. Ongoing research efforts aim to address this limitation, focusing on enhancing the adaptability of implicit geometric and variational level set methods to diverse image characteristics for more robust and accurate segmentation outcomes. [26]–[28].

The concept of implicit variational level set methods has been applied effectively within the realm of local region-based active contours (AC), offering a tailored approach to image processing and computer vision challenges. Several models, including LRBAC (Local Region-Based Active Contour), LBF (Local Binary Fitting), LIF (Local Intensity Fitting), LIC (Local Intensity and Contrast), LSAC (Local Shape-Constrained Active Contour), LCV (Local Color Variance), LRCV (Local Region-Based Color Variance), LGDF (Local Gradient Direction Fitting), and LLIF (Local Level Set with Intensity Fitting), exemplify the diversity within this category. These models contribute significantly by

localizing contours to adapt to heterogeneous image conditions, demonstrating effectiveness in scenarios where a more nuanced approach is required. It is important to acknowledge certain weaknesses inherent in these methods, such as the potential for excessive convolution operations, resulting in models that are computationally heavy and slow. Addressing these computational challenges remains a focal point for researchers seeking to enhance the efficiency and applicability of implicit variational level set models in local region-based active contour applications. [29]–[31].

The concept of implicit geometric and variational level set methods has been ingeniously applied in the domain of hybrid active contours (AC), offering a synthesis of both local and global strategies for image processing and computer vision challenges. Various models, including GACV (Global and Local Geometric Active Contour with Vectors), LGBF (Local and Global Binary Fitting), GLIF (Global and Local Intensity Fitting), LGGDF (Local and Global Gradient Direction Fitting), and SPFLBF (Sparse Field Level Set with Local Binary Fitting), exemplify the diversity within this hybrid category. These models make noteworthy contributions by seamlessly integrating local and global AC components, providing a more adaptable and robust framework for contour evolution. It's important to recognize certain weaknesses associated with these hybrid models, such as a higher degree of intervention required during parameter tuning and a notable computational cost, which can be burdensome in resource-intensive applications. Researchers are actively addressing these challenges to strike a balance between intervention and computational efficiency, aiming to further enhance the versatility and practicality of implicit geometric and variational level set methods in the context of hybrid active contour models. [32]–[34].

Human skills in manually annotating the investigated US images are certainly competent and careful. However, the need for high reproducibility and efficiency in performing this task motivates the development of automatic segmentation methods. This study aims to develop an AC model that can be used as an effective segmentation method on US images in the field of radiology. This effort is categorized into two specific objectives. (1) Developing a hybrid AC formulation that is capable of working autoadaptive to the character of US image so that operator intervention can be minimized. (2) Integrating the proposed hybrid AC model with morphological Gaussian-based regularization to maintain evolutionary stability and handle inhomogeneity.

By achieving an autoadaptive AC segmentation technique in this study, the radiologists gained three benefits i.e. accurate local detection of investigated objects, more efficient CAD procedure and its practical use with minimal intervention.

The structure of this paper is as follow: after explaining the background, research gaps, and study objectives in Introduction, a review and theoretical basic of AC based segmentation is describe in Literatur Reviews. Next, the method developed in this study is described in the Methodology. The results of the testing and validation of the method are explained in the Results and Discussion. Lastly, Conclusion is described about summarizes and concludes the study.

2. Literatur Reviews

This study utilizes a hybrid model to develop a new automated segmentation method by leveraging both the local edge-based geodesic active contour (GAC) model and the global region-based Chan-Vese model.

2.1 Edge-based GAC

After the development of implicit geometric AC models based on the level set theory [35] by Caselles et al. [36] and Malladi et al. [37], explicit parametric AC models are rarely used. The segmentation mechanism is then represented as a solution to a partial differential equation obtained implicitly at the zero level set (ZLS) condition. The level set formulation allows the AC curve to reliably handle merging and splitting in dynamic object topology. Additionally, multiple objects can be segmented simultaneously in a single evolution using the same initial contour. The evolution is halted by an edge stopping function (ESF) obtained through edge gradient after smoothing operations. AC segmentation techniques with optimized ESF like this are specifically known as edge-based models. The most fundamental example of an edge-based AC model is the Geodesic Active Contour (GAC) by Caselles et al. [38]. The GAC model uses edge information of the image, which makes the model sensitive to noise and clutter, which will lead boundary leak phenomenon to the segmentation result, at the same time, the model is highly sensitive to the initial contour position.

In general, the main drawback of edge-based models is their high dependence on the effectiveness of the ESF (edge stopping function). The intervention of operators in determining the

smoothing parameters and the initial contour location still relies on trial and error. GAC often gets trapped in the local minimum (LM) area due to inaccurate initial contour placement. Excessive smoothing operations can also lead to the loss of object edge sharpness, resulting in leakage issues.

2.2 Simplified CV

Due to these limitations, Chan-Vese (CV) [24] subsequently developed the Active Contour Without Edge (ACWE) based on the curve evolution theory of Mumford-Shah [105], represented in the concept of variational level set. This model works globally, similar to clustering, as it investigates the entire object in an image field. It is known as a "variational" model because of the fundamental modifications made to the general level set evolution equation (LSE). The CV model utilizes the mean intensity between the foreground and background as a suitable term to stop the evolution. The fitting term replaces the ESF in edge-based models. In addition to being reliable in segmenting blurred objects, the CV model is also insensitive to the initial contour placement. Regardless of the initial contour's position, the curve continues to evolve towards the object edges based on the obtained average intensity values. It has been discovered that the global region-based concept is only optimal for homogeneous foreground and background regions. In cases of inhomogeneity, the AC curve becomes trapped in the false attractor (FA) regions.

2.3 Similar Studies

The use of AC models as a method of segmenting US images was found in several studies summarized in Table 1. Of these studies, breast lesions and thyroid nodules are the most discussed objects. Thyroid and breast cancer are two malignancies with the highest incidence in women [39]. Epidemiological studies have shown that patients with breast cancer have a higher risk of developing thyroid cancer, and vice versa [40], [41]. Therefore, both cancers may share some similarities, such as hormonal factors, genetic predisposition, environmental factors, and related therapies [42]. To help reduce the number of deaths due to cancer, an innovation is needed to assist radiologists in diagnosing cancer, especially to expedite the screening process by automating it. The US imaging of breast and thyroid cancer can be seen in Figure 5.

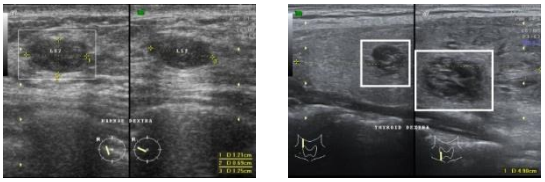

(a) (b)

Figure 5. US images (a) of breast cancer and (b) of thyroid cancer.

This study designedly involved the two types of cancer objects to obtain sufficient datasets capable of representing other similar radiological objects. With the adequacy of existing datasets, the performance evaluation of the proposed AC model becomes increasingly valid and significant. Meanwhile, previous studies were limited to one kind of US object only.

Table 1. Utilization of the AC models for US image segmentation.

Study	Object	Model
[43]–[48] [49] [50] [19], [51], [52]	- Breast - Thyroid - Liver - Artery	*Snakes* [22]
[53] [14], [54]–[56]	- Breast - Thyroid	GAC* [53]
[4], [57]–[61] [4], [11], [70]–[76], [62]–[69] [77] [78]	- Breast - Thyroid - Liver - Heart	CV** [79]
This paper	- Breast & thyroid	Hybrid CV-GAC

*GAC = *Geodesic Active Contour*, **CV = *Chan-Vese*

Additionally, several studies leverage AC for the development of CAD systems.

In 2015, Nugroho et al. conducted a study developing a method called ACBF (Active Contour Bilateral Filter) for breast lesion segmentation in ultrasound (US) images [60]. The bilateral filter was used in the study to reduce speckle noise in US images. The ACBF method combines active contour segmentation with the bilateral filter to separate the breast lesion area. The research findings showed that using this method could detect the edges of breast lesions, iteratively separate normal tissues, and successfully reduce noise in US images. The testing results using parameters such as MSE (Mean Square Error), SNR (Signal to Noise Ratio), PSNR (Peak Signal to Noise Ratio), AD (Average Difference), and SI (Speckle Index) yielded the following respective values: 38.90324, 21.25934, 32.23095, 0.019258, and 7.77e-6.

In 2020, Nugroho et al. conducted further research by developing the ACBF method [4]. The method evolved into a Combinatorial Active Contour Bilateral Filter. The study presented a

combinatorial framework for US image segmentation using the bilateral filter (BF) and a Region-Edge-based AC model. The research findings showed a Dice coefficient value of 90.05 ± 5.81% with a dataset consisting of 258 US images along with their ground truth annotations.

In the same year, Nugroho et al. also conducted research by developing a method called MoRbAC (Morphological Region-based Active Contour) for automatic cancer object detection in US images [4]. The study was implemented on four samples of breast and thyroid cancer US images. The average values from each validation were as follows: accuracy of 98.58±0.89%, sensitivity of 89.58±7.69%, specificity of 99.58±0.11%, precision of 95.58±2.77%, and similarity of 92.36±4.67%. In conclusion, the high performance of MoRbAC demonstrates its potential for practical applications in the development of computer-aided detection (CAD) systems.

The MoRbAC method was further implemented in a study titled "Ultrasound object detection using morphological region-based active contour: an application system" [80]. The results of the research demonstrated that the MoRbAC (Morphological Region-Based Active Contour) method worked well in program implementation and was tested on 20 US images of breast cancer lesions and thyroid nodules. Quantitative measurements based on the overlapping area compared to the referenced ground truth achieved an average accuracy of up to 98.58 ± 1.15% with a relatively short average execution time of 2.38 ± 0.89 seconds. This promising performance concludes the effectiveness and efficiency of MoRbAC as a viable method to be applied in computer-aided detection (CAD) systems.

In 2022, the CV method was simplified by Nugroho et al. for cancer object detection in US images [81]. The simplified CV, followed by morphological operations, proved to be effective in object detection by achieving quantitative performance measured using Intersection over Union (IoU) scores between the detected objects and their ground truth annotations. The proposed method was validated using 20 thyroid and breast US images, resulting in an average IoU score of 92.36%. This promising performance indicates that the proposed method is suitable for implementation in CAD systems. In 2023, Nugroho et al. implemented the MoRbAC method, which includes a simplified CV model, within a web-based application [82]. The proposed web-based application has been validated on 20 breast lesion and thyroid nodule US images. Python programming with the Flask framework was used to deploy this application. The validated results are compatible with various browsers and achieve an average accuracy of 98.75%. This achievement demonstrates that MoRbAC is suitable for use as an US CAD detection technique in a web service system.

This work can be considered as an extension of the MoRbAC method that was previously developed. The MoRbAC method is limited to carrying out automatic detection with bounding box output for suspected cancer objects but has not yet completed it to the segmentation stage. The detection process serves as a preprocessing stage in the CAD system, which is still in its early phase. Meanwhile, the proposed method here is already capable of performing the segmentation process. The segmentation process is a crucial stage in the CAD system, providing a wealth of information for the feature extraction and classification stages, thereby obtaining accurate diagnostic results.

3. Methodology

3.1 Dataset

In this study, the dataset consists of 50 US images, comprising 35 breast cancer object images and 15 thyroid gland images obtained from the Department of Radiology, Dr. Sardjito General Hospital, and Hardjolukito Air Force Hospital in Yogyakarta, Indonesia. All types of nodules and lesions exhibit diverse features for classification into benign and malignant categories. However, these features do not affect the segmentation process, as the segmentation results will be used to extract these features afterward. As they are acquired from the same machine, the image quality and noise levels are consistent across all datasets. The images are available in .png format and accompanied by ground truth data, which can be used to validate the segmentation results obtained through a Python program.

3.2 ACAC Segmentation Method

The Automatic Combinatorial Active Contour (ACAC) is a method developed in this study for automatic segmentation in US image. This method combines CV (Chan-Vese) models for global segmentation and GAC (Geodesic Active Contour) for accurate local segmentation. The method is automated and applied to object detection to generate initial contour results through the simplification of the CV formulation.

The segmentation of US images through the ACAC method is carried out through the following process. First, the ESF (becoming to

Binary Stopping Function-BSF) is created using the simplified CV formulation, followed by local object delineation using GAC. ACAC combines the simplified CV model in equation (1) with the GAC model in equation (2).

$$\frac{\partial \emptyset}{\partial t} = \left[div\left(\frac{\nabla \emptyset}{|\nabla \emptyset|}\right) + [I - 0.5(c_1 + c_2)\right] \delta(\emptyset) \quad (1)$$

$$\frac{\partial \emptyset}{\partial t} = \left[div\left(g\frac{\nabla \emptyset}{|\nabla \emptyset|}\right) + vg\right] \quad (2)$$

where:

ϕ = level set function
t = time variable
div = divergence operation
∇ = spatial gradien function
I = Input image
c_1 = average pixel value in the contour
c_2 = average pixel value out of the contour
δ = dirac function
g = ESF (Edge Stopping Function)
v = constant velocity.

From the combination of the two equations, the ACAC formulation is obtained as follows:

$$\frac{\partial \emptyset}{\partial t} = \left\{div\left(\kappa\frac{\nabla \emptyset}{|\nabla \emptyset|}\right) + (1 - |\alpha|)\left[I - \frac{c_1 + c_2}{2}\right] + \alpha\kappa\right\}|\nabla \emptyset| \quad (3)$$

where κ = *curvature*.

The main process of the ACAC method is illustrated in Figure 65.

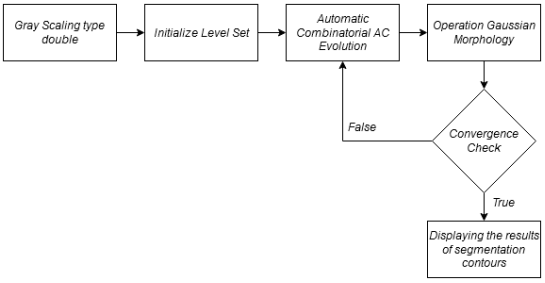

Figure 6. ACAC Method Process.

3.2.1 Grayscalling

First step is grayscalling. It is the initial step to convert the data of each pixel in the US image into a single channel that has values ranging from 1 to 225, with a data type of double (which can store decimal and negative values) based on the level of light intensity in the image.

3.2.2 Initialize Level Set (ϕ_0)

Secound step is initialize level set. This is the process of initializing the starting position of the curve evolution in the US image. The initialization location is typically set at the center of the image to be detected, requiring the width and height parameters of the image I(x, y). In this step, a binary image will be generated, which means an image that only has two values: 0 and 255. The initialization of the level set is performed using the following equation.

$$\phi_0 = \phi_0(x, y, 0) = \begin{cases} -1, jika\ (x, y) \in C_0 \\ 1, jika\ (x, y) \notin C_0 \end{cases} \quad (4)$$

where C_0 represents the initialization region within the domain of the image I(x,y).

3.2.3 ACAC Evolution

The third step is ACAC evolution. It is a series of evolution processes implemented using the ACAC formulation in equation (3). The evolution process in this stage is illustrated in Figure 7 below.

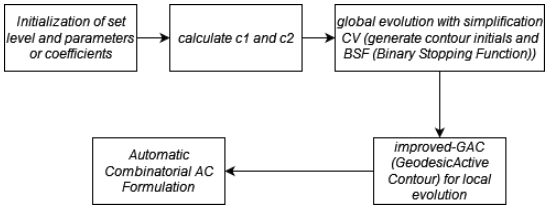

Figure 7. ACAC Evolution Process.

Basically, the CV method is a global segmentation method, meaning the initial contour can be placed anywhere in the image field. The CV method will automatically evolve the contour, regardless of the initial contour's specific location. The ACAC method is designed to operate automatically without manual adjustments, resulting in the following level set evolution equation:

$$\frac{\partial \phi}{\partial t} = \left(I - \frac{c_1 + c_2}{2}\right) \quad (5)$$

Where the constant c_1 represents the average intensity inside the curve, and c_2 represents the average intensity outside the curve, which can be obtained through the following formulation:

$$\begin{cases} c_1(\phi) = \frac{\iint I(x,y).H(\phi)\, dxdy}{\iint H(\phi)\, dxdy}, \phi < 0 \\ c_2(\phi) = \frac{\iint I(x,y).(1-H(\phi))\, dxdy}{\iint (1-H(\phi))\, dxdy}, \phi > 0 \end{cases} \quad (6)$$

$H(\phi)$ is the Heaviside function formulated as follows:

$$H(\phi) = \frac{1}{\pi}\tan^{-1}(\phi) + 0.5 \quad (7)$$

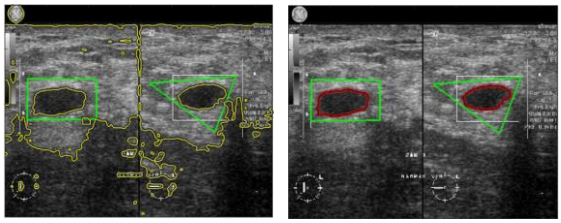

(a) (b)

Figure 8. Ilustration (a) global evolution, (b) and local evolution [83].

In equation (3), the parameters κ and α play a role in controlling the transition between global and local evolution (switching control). The evolution process in the ACAC method is performed through two stages of evolution. First, global evolution is carried out to automatically detect all objects in the image, regardless of the location of the initialization, as shown in Figure 8 point a, where the green contour represents the initial contour and the yellow contour represents the final contour. Second, local evolution is performed for more specific object segmentation. Convergence checking is conducted for each result of global and local evolutions, preceded by a morphological operation stage.

3.2.4 Operation Gaussian Morphologhy

In the ACAC method, two morphological operations, namely opening and closing, are performed on the ACAC-evolved image. These operations are convolved with a Gaussian kernel to suppress artifacts and speckles, thereby effectively preventing leakage, LM, and FA. In US segmentation, adopting Gaussian filtering is quite reasonable as it gives smoothing effect to suppress speckle and artifact. This process also helps accelerate the convergence of evolution.

With these sequential opening and closing, small foregrounds are not considered in the segmentation process and therefore the ACAC algorithm becomes robust to noisy images. This morphological-Gaussian provides an advantage to suppress speckles and artifacts so that the inhomogeneity of US images can be overcome. This regularization also eliminates preprocessing so that CAD works in shorter and more efficient stages.

3.2.5 Checking Convergence

Convergence is a parameter in AC evolution that indicates decreasing error and leads to the contour stopping at the desired segmentation target. The convergence mechanism, as an Evolution Stopping Criterion (ESC) control, is implemented to make the method automatic based on the criteria given in Equation (8) and Equation (9). With this approach, the transition from global to local segmentation can be performed automatically. Bear in mind that ESC converges twice. Keep on calculating ErrorLength and ErrorArea during iteration until after both are less than or equal to θ then switch global evolution mode to local at the first convergence. Where θ being a tolerable small number. Go back to step 3, which is ACAC Evolution, until ESC converges for the second one, then evolution ACAC breaks.

$$\text{Error Length} = Length\ (\phi^{i+1}) - Length\ (\phi^{i}) \leq \theta \quad (8)$$

$$\text{Error Area} = Area\ (\phi^{i+1}) - Area\ (\phi^{i}) \leq \theta \quad (9)$$

3.2.6 Display the Results

After the result has converged, the segmentation outcome will be displayed, showing the segmented contour. This outcome can then be tested and analyzed further.

3.3 Testing Method and Validation

The testing and validation method used in the research is the confusion matrix. The confusion matrix provides information about how often certain behaviors are detected correctly and how often they are classified as other behaviors [84]. This data analysis method is used to compare the results of automatic segmentation of cancer objects with the manual ground truth created by radiologists. The research uses seven (7) indicators, including accuracy, precision, sensitivity, specificity, similarity, Intersection over Union (IoU) score, and CPU time.

In Figure 9, the segmented object is marked in red, while the ground truth is marked in green, overlapping each other to obtain the values of TP, TN, FP, and FN used for validating the accuracy, precision, sensitivity, specificity, and similarity using Equations (10)-(14). High percentage values of accuracy, precision, sensitivity, specificity, and similarity indicate that the segmented contour closely matches the ground truth.

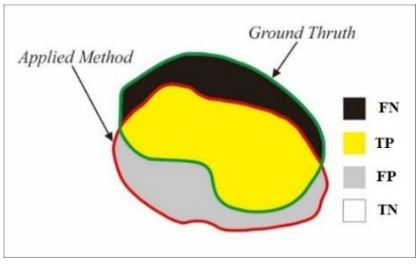

Figure 9. Testing and validation using confussion matrix.

$$\text{Accuracy} = \frac{|TP+\text{TN}|}{|TP+\text{FP}+\text{FN}+\text{TN}|} \times 100\% \quad (10)$$

$$\text{Precission} = \frac{|TP|}{|TP+\text{FP}|} \times 100\% \quad (11)$$

$$\text{Sensitivity} = \frac{|TP|}{|TP+\text{FN}|} \times 100\% \quad (12)$$

$$\text{Specifity} = \frac{|TN|}{|TN+\text{FP}|} \times 100\% \quad (13)$$

$$\text{Similarity} = \frac{|2TP|}{|2TP+\text{FP}+\text{FN}|} \times 100\% \quad (14)$$

IoU (Intersection over Union) is the overlapping area between the predicted segmentation and the ground truth divided by the combined area of the predicted segmentation and the ground truth. equation (15) represents the calculation of IoU.

$$\text{IoU} = \frac{TP}{FN+TP+FP} \times 100\% \quad (15)$$

CPU-Time (or CPU-usage, runtime) is the amount of time the CPU requires to process computer program instructions (excluding waiting time for input/output operations).

The testing was conducted by developing a specialized Python program to calculate the difference in the number of pixels between the manually created groundtruth and the proposed method's results. The pixels in the binary image resulting from the ACAC method's segmentation were counted using the NumPy and OpenCV libraries and then processed according to Equations (10)-(15).

4. Results and Discussion

In this study, the cancer dataset obtained consists of images with a gray-level depth of 256. The lesions in the dataset were clinically analyzed by radiologists, and manual segmentation was provided as groundtruth. The collected dataset consists of various forms of nodules or lesions. In a single image, there may be one or more detected nodules or lesions. One of the datasets used is shown in Figure 10.

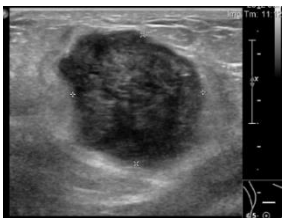

Figure 10. Example of US image dataset.

Next, the ACAC method algorithm will be applied to US images. This method will automatically detect the location of the cancer using level set initialization. The initial level set location will detect the length and width of the cancer object, and then the level set will shrink following the contours of the cancer object. This process minimizes local minima and leakage on weakly defined edge boundaries of the object.

The initial step before image processing (preprocessing) is Grayscaling, which converts each pixel in the image into a single channel with values ranging from 0 to 255 based on the intensity level of the light. Then, the level set initialization is performed to initialize the starting point of the curve evolution in an image. The initialization point is typically set at the center of the image to be detected, requiring parameters for the width and height of the image I(x, y), as shown in Figure 11. In the figure, white color corresponds to a value of 1, while black color corresponds to a value of 0.

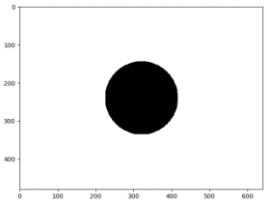

Figure 11. Initialize level set.

Next, the regularization of the ACAC algorithm is performed. By utilizing the CV simplification for global segmentation, the regularization process produces a bounding box that functions as the detection of the cancer location. Before generating the bounding box, the regularization starts by applying the ACAC formula in the program, resulting in an image similar to Figure 12 point (a).

Next, a binary procedure is applied using Gaussian morphological operations, followed by morphological operations such as opening, clearing borders, and filling holes. These series of morphological operations are performed to reduce noise in the image, and the binary procedure is applied to obtain the processed image result as shown in Figure 12 point (b).

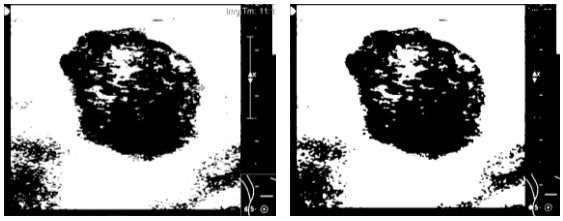

(a) (b)

Figure 12. Sample image result of (a) regularization process and (b) Binary Gaussian procedure.

After detecting all the objects in the image, each connected pixel is labeled to form objects that are suspected to be cancerous. This step allows for obtaining region properties for each object using the regionprops function. Each suspected cancerous object is marked with a bounding box, with a tolerance of 20 pixels at each corner, as shown in Figure 13, which also indicates the result of the first iteration.

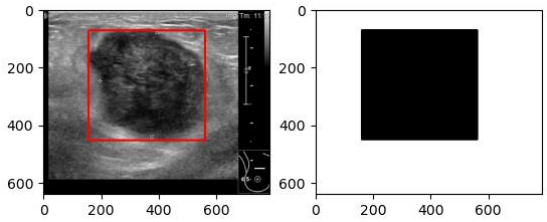

Figure 13. Detection cancer object sample image result.

After the cancerous objects are detected by the bounding box, the next step is to perform iterations by applying the improved-GAC method to achieve accurate local segmentation. The bounding box (red contour) acts as the level set, which then segments the object using the shrinking method, following equation (16) below.

$$\kappa \begin{cases} H(\phi) & expanding\ GAC, v < 0\ and\ C_0 \\ 1 - H(\phi) & shrinking\ GAC, v > 0\ and\ C_0 \end{cases} \quad (16)$$

The iteration process will continue until the level set approaches a value of 0. Once it reaches this condition, the iteration will stop, and the segmentation process will end. The segmentation result with the given input image sample is shown in Figure 14.

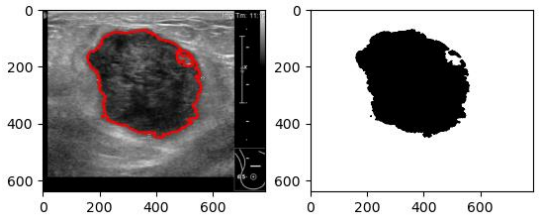

Figure 14. Segmentation cancer object sample image result.

Based on the overlapping area between the automatically segmented result and the manually created ground truth by radiologists. This overlapping area will indicate the values of TP, TN, FP, and FN. The visualization of these values can be seen in Figure 15.

Figure 15 shows eight different visualizations of the confusion matrix values used. BW represents the image resulting from automatic segmentation using the ACAC method. GT represents the manually created ground truth image. SA represents the combined area between BW and GT. TP (True Positive) is the area BW ∩ GT, while TN (True Negative) is ~BW ∩ ~GT. FN (False Negative) is ~BW ∩ GT, FP (False Positive) is BW ∩ ~GT, and FA is inversely related to SA. The values of the confusion matrix are obtained from the number of white pixels in the image area.

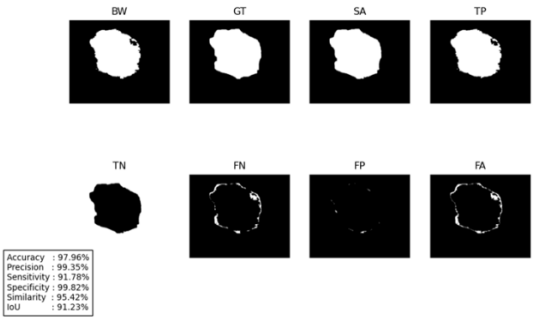

Figure 15. Testing segmentation sample image result using confusion matrix method.

Based on these values, several dice coefficient calculations were obtained to validate the testing of accuracy, precision, sensitivity, specificity, similarity, and intersection over union. Each dataset will have a dice coefficient value and CPU time, which is used to determine how fast the automatic segmentation process is on US images.

Figure 16 point a-g depict graphs of the test results for each validation test on 50 datasets. The accuracy percentages range from a minimum of 96.33% to a maximum of 99.94%. The precision percentages vary from a minimum of 86.47% to a maximum of 99.78%. The lowest sensitivity is at 75.06%, while the highest is at 95.9%. Specificity ranges from 97.17% to 100%. The similarity percentages vary from a minimum of 84.91% to a maximum of 95.42%. The IoU percentages range between 73.77% and 91.23%. The fastest CPU time is recorded at 6.47 seconds, while the slowest is at 188.83 seconds.

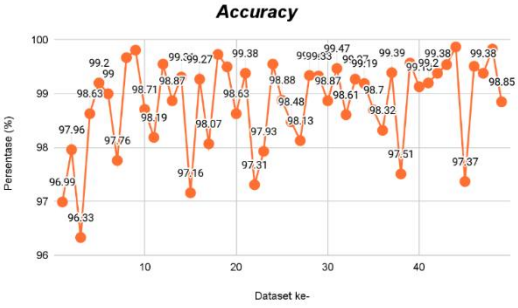

(a)

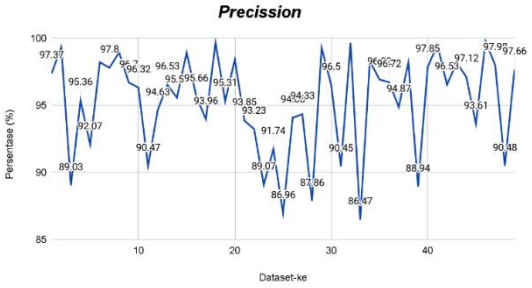

(b)

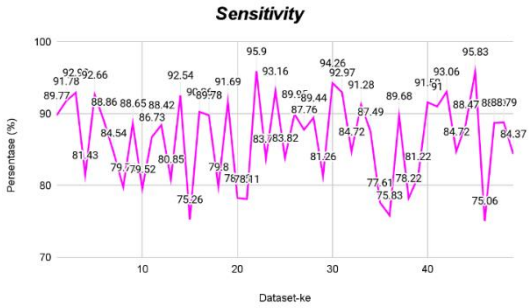

(c)

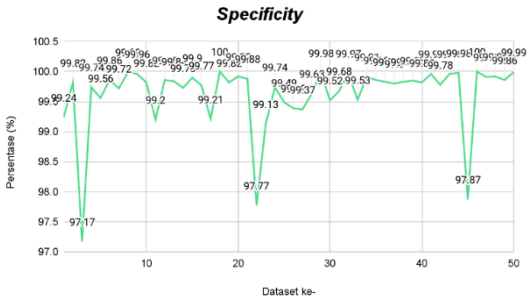

(d)

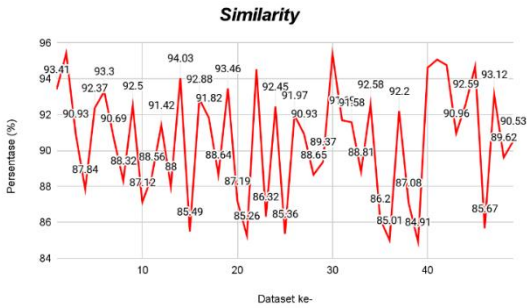

(e)

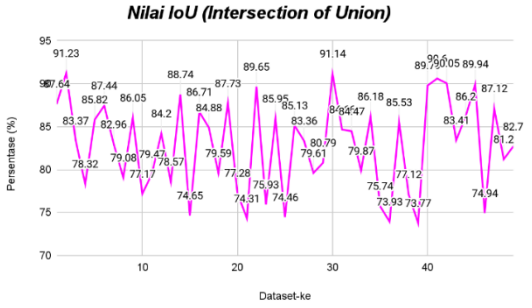

(f)

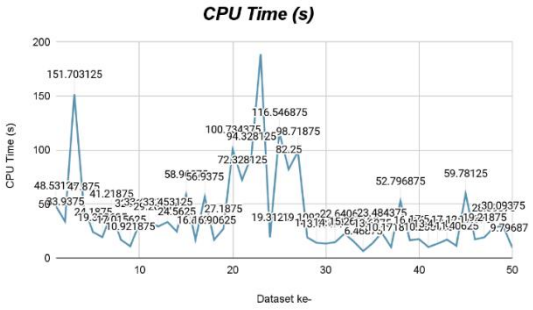

(g)

Figure 16 (a-g). Graph showing the result for each indicators testing using 50 datasets.

Table 2. Summary of the results of the calculation of the validity test.

Indicators	Min.	Max.	Average
Accuracy	96.33%	99.94%	98.8314%
Precision	86.47%	99.78%	95.2646 %
Sensitivity	75.06%	95.9%	86.5842%
Specificity	97.17%	100%	99.6268 %
Similarity	84.91%	95.42%	90,547%
IoU	73.77%	91.23%	82.874 %
CPU Time	6.47 s	188.83 s	39.09 s

Table 2 shows the values generated from the calculation of the dice coefficient of the 50 datasets used in this study. From the entire dataset, the automatic segmentation process is fast because it only takes about 39.09 seconds. The accuracy level of this method is very high, as indicated by the average calculation above, which is 98.83%. The precision level, which indicates the accuracy of pixel detection, is 95.26%. The average sensitivity value obtained is 86.58%, indicating a high ability to detect cancer object pixels. The average specificity value obtained is 99.63%. The similarity value has an average of 90.58%, and the average IoU value obtained is 82.87%. The IoU value is used to determine the suitability of the automatic segmentation area with the manual ground truth, and the value obtained is considered quite high in the ACAC method in this research.

The high variability in the quality of US images results in reduced image contrast. Additionally, uneven pixel intensity causes objects to appear blurry. These weaknesses make the interpretation process of US images still subjective. The development of Computer-Aided Diagnosis (CAD) as a second opinion simplifies the interpretation process. However, some machines still require manual initialization of the cancer object's location and the selection of desired segmentation results. This is ineffective

and increases the likelihood of human error, especially when repeated for a large number of patients. With the ACAC method developed in this work, the interpretation process becomes more efficient and reduces the chances of human error. The manual initialization aspect has been eliminated with this proposed ACAC model. Furthermore, the preprocessing stage has been integrated with the automatic segmentation model, allowing the elimination of the preprocessing stage and thus shortening the process in CAD. However, the ACAC model has not been directly tested as CAD in the US machine. Therefore, in this study, the model cannot conclude the type of detected cancer, whether benign or malignant. Further work is needed to extract features and classify them in the CAD system sequence to obtain accurate diagnostic results.

5. Conclusion

Based on the results and discussion, it shows that the AC model has a potential and ability to be developed as an effective segmentation method for radiological US images. This study successfully developed an automatic cancer object segmentation method on US images to assist radiologists in the efficient diagnosis process called Automatic Combinatorial Active Contour (ACAC). The method was implemented in a Python program to perform segmentation of thyroid and breast cancer objects.

The high level of intervention or operator dependence on the AC model has been overcome by developing of a hybrid edge and region based active contour model called ACAC that is enriched with autoadaptive capabilities i.e automation and adaptability. The binary stopping function (BSF) has been successfully utilized as an automatic lesion detector eleminating manual initialization.

The proposed Morphological Gaussian-based regularization which is integrated into the ACAC model has succeeded in maintaining evolutionary stability and dealing with the inhomogeneity of speckled and artifacted US images. The occurrence of problematic FA, leakage, and LM has been able to be overcome without the need for preprocessing efforts.

Furthermore, the accuracy level of this method is very high, as seen from the average calculation above, which is 98.83%. Therefore, the ACAC method is worthy of implementation in CAD systems to obtain accurate diagnosis results and more objective clinical recommendations.

Apart from practicality, an efficient segmentation process is a necessity in radiological CAD system. The improvement in ACAC efficiency is an issue that is highly recommended for further task. Automated object detection techniques for initial contour determination that do not involve many iterative operations need to be considered. The watershed method and some clustering techniques also have the potential to be utilized, considering that they have the same type of global segmentation as the CV model. The completeness of the US image dataset, apart from breast and thyroid cancer, is an invaluable support in this study. The performance of the proposed ACAC needs to be more comprehensively validated on more varied cancer objects. The consequence of adding a dataset will also increase the work of radiologists to make ground truth. Also with the increasing variety of cancer objects, there may be a number of objects that have significant ground truth differences between radiologists.

Acknowledgement

This research is part of the Basic Research funded by DIPA, Faculty of Engineering, State University of Semarang. The authors would like to thank Dr. Lina Choridah, Sp. Rad. and her mentored students in the Department of Radiology, Faculty of Medicine, Universitas Gadjah Mada for providing the dataset of radiological US images including the ground truth and for all of the valuable discussions during this research. We also thank UNNES colleagues, especially colleagues in the AIRIoT (Artificial Intelligent, Robotic and Internet of Things) Lab at the UNNES Digital Center building, who have provided space, insight, and expertise that really helped this work.

References

[1] A. Rodríguez-Cristerna, W. Gómez-Flores, and W. C. de Albuquerque Pereira, ‘A computer-aided diagnosis system for breast ultrasound based on weighted BI-RADS classes’, *Comput. Methods Programs Biomed.*, vol. 153, pp. 33–40, 2017, doi: 10.1016/j.cmpb.2017.10.004.

[2] T. L. Szabo, *Diagnostic Ultrasound Imaging: Inside Out*. Elsevier, 2014. doi: 10.1016/C2011-0-07261-7.

[3] R. Takahashi and Y. Kajikawa, ‘Computer-aided diagnosis: A survey with bibliometric analysis’, *Int. J. Med. Inform.*, vol. 101, pp. 58–67, 2017, doi: 10.1016/j.ijmedinf.2017.02.004.

[4] A. Nugroho, R. Hidayat, H. Adi Nugroho, and J. Debayle, ‘Cancerous object detection using morphological region-based active contour in ultrasound images’, *J. Phys. Conf. Ser.*, vol. 1444, no. 1, 2020, doi: 10.1088/1742-6596/1444/1/012011.

[5] W. Gómez-Flores and B. A. Ruiz-Ortega, ‘New fully automated method for segmentation of breast lesions on ultrasound based on texture analysis’, *Ultrasound Med.*

Biol., vol. 42, no. 7, pp. 1637–1650, 2016, doi: 10.1016/j.ultrasmedbio.2016.02.016.

[6] S. Wu, Q. Zhu, and Y. Xie, 'Evaluation of various speckle reduction filters on medical ultrasound images', *Proc. Annu. Int. Conf. IEEE Eng. Med. Biol. Soc. EMBS*, pp. 1148–1151, 2013, doi: 10.1109/EMBC.2013.6609709.

[7] N. S. Narayan, P. Marziliano, and C. G. L. Hobbs, 'Automatic removal of manually induced artefacts in ultrasound images of thyroid gland', *Proc. Annu. Int. Conf. IEEE Eng. Med. Biol. Soc. EMBS*, pp. 3399–3402, 2013, doi: 10.1109/EMBC.2013.6610271.

[8] M. I. Samsung, 'Ultrasound: S Detect for Thyroid RS80', 2016. https://www.youtube.com/watch?v=Syu4NjD2qwA

[9] E. Y. M. SA, 'RS80A S Detect Categorization for breast', 2015. https://www.youtube.com/watch?v=gfw5Qex6Ln8

[10] J. A. Noble, 'Ultrasound image segmentation and tissue characterization', *Proc. Inst. Mech. Eng. Part H J. Eng. Med.*, vol. 224, no. 2, pp. 307–316, 2010, doi: 10.1243/09544119JEIM604.

[11] Zulfanahri, H. A. Nugroho, A. Nugroho, E. L. Frannita, and I. Ardiyanto, 'Classification of thyroid ultrasound images based on shape features analysis', *BMEiCON 2017 - 10th Biomed. Eng. Int. Conf.*, vol. 2017-Janua, pp. 1–5, 2017, doi: 10.1109/BMEiCON.2017.8229106.

[12] A. Nugroho, R. Hidayat, and H. A. Nugroho, 'Artifact removal in radiological ultrasound images using selective and adaptive median filter', *ACM Int. Conf. Proceeding Ser.*, pp. 237–241, 2019, doi: 10.1145/3309074.3309119.

[13] S. Bohlender, I. Oksuz, and A. Mukhopadhyay, 'A Survey on Shape-Constraint Deep Learning for Medical Image Segmentation', *IEEE Rev. Biomed. Eng.*, vol. 16, pp. 225–240, 2023, doi: 10.1109/RBME.2021.3136343.

[14] D. Koundal, S. Gupta, and S. Singh, 'Automated delineation of thyroid nodules in ultrasound images using spatial neutrosophic clustering and level set', *Appl. Soft Comput.*, vol. 40, pp. 86–97, Mar. 2016, doi: 10.1016/J.ASOC.2015.11.035.

[15] H. D. Cheng, J. Shan, W. Ju, Y. Guo, and L. Zhang, 'Automated breast cancer detection and classification using ultrasound images: A survey', *Pattern Recognit.*, vol. 43, no. 1, pp. 299–317, Jan. 2010, doi: 10.1016/J.PATCOG.2009.05.012.

[16] S. Sridevi and M. Sundaresan, 'Survey of image segmentation algorithms on ultrasound medical images', *Proc. 2013 Int. Conf. Pattern Recognition, Informatics Mob. Eng. PRIME 2013*, pp. 215–220, 2013, doi: 10.1109/ICPRIME.2013.6496475.

[17] M. Xian, Y. Zhang, H. D. Cheng, F. Xu, B. Zhang, and J. Ding, 'Automatic breast ultrasound image segmentation: A survey', *Comput. Vis. Pattern Recognit.*, pp. 10–71, Jul. 2017, doi: 10.1016/J.PATCOG.2018.02.012.

[18] Q. Huang, Y. Luo, and Q. Zhang, 'Breast ultrasound image segmentation: a survey', *Int. J. Comput. Assist. Radiol. Surg.*, vol. 12, no. 3, pp. 493–507, 2017, doi: 10.1007/s11548-016-1513-1.

[19] K. M. Meiburger, U. R. Acharya, and F. Molinari, 'Automated localization and segmentation techniques for B-mode ultrasound images: A review', *Comput. Biol. Med.*, vol. 92, pp. 210–235, 2018, doi: 10.1016/j.compbiomed.2017.11.018.

[20] A. Nugroho, R. Hidayat, and H. A. Nugroho, 'Thyroid ultrasound image segmentation: A review', *Proc. - 2019 5th Int. Conf. Sci. Technol. ICST 2019*, 2019, doi: 10.1109/ICST47872.2019.9166443.

[21] E. N. K. Kollorz, D. A. Hahn, R. Linke, T. W. Goecke, J. Hornegger, and T. Kuwert, 'Quantification of thyroid volume using 3-D ultrasound imaging', *IEEE Trans. Med. Imaging*, vol. 27, no. 4, pp. 457–466, 2008, doi: 10.1109/TMI.2007.907328.

[22] M. Kass, A. Witkin, and D. Terzopoulos, 'Snakes: Active contour models', *Int. J. Comput. Vis.*, vol. 1, no. 4, pp. 321–331, 1988, doi: 10.1007/BF00133570.

[23] V. Caselles, R. Kimmel, and G. Sapiro, 'Geodesic Active Contours', *Int. J. Comput. Vis.*, vol. 22, no. 1, pp. 61–79, 1997, doi: 10.1023/A:1007979827043.

[24] T. F. Chan and L. A. Vese, 'Active contours without edges', *IEEE Trans. Image Process.*, vol. 10, no. 2, pp. 266–277, 2001, doi: 10.1109/83.902291.

[25] L. D. Cohen, 'On active contour models and balloons', *CVGIP Image Underst.*, vol. 53, no. 2, pp. 211–218, 1991, doi: 10.1016/1049-9660(91)90028-N.

[26] K. Zhang, L. Zhang, H. Song, and W. Zhou, 'Active contours with selective local or global segmentation: a new formulation and level set method', *Image Vis. Comput.*, vol. 28, no. 4, pp. 668–676, 2010.

[27] J. Piovano, M. Rousson, and T. Papadopoulo, 'Efficient segmentation of piecewise smooth images', *Lect. Notes Comput. Sci. (including Subser. Lect. Notes Artif. Intell. Lect. Notes Bioinformatics)*, vol. 4485 LNCS, pp. 709–720, 2007, doi: 10.1007/978-3-540-72823-8_61.

[28] J. An, M. Rousson, and C. Xu, 'Γ-Convergence approximation to piecewise smooth medical image segmentation', *Lecture Notes in Computer Science (including subseries Lecture Notes in Artificial Intelligence and Lecture Notes in Bioinformatics)*, vol. 4792 LNCS, no. PART 2. pp. 495–502, 2007. doi: 10.1007/978-3-540-75759-7_60.

[29] K. Zhang, L. Zhang, K. M. Lam, and D. Zhang, 'A Level Set Approach to Image Segmentation with Intensity Inhomogeneity', *IEEE Trans. Cybern.*, vol. 46, no. 2, pp. 546–557, 2016, doi: 10.1109/TCYB.2015.2409119.

[30] X. F. Wang, D. S. Huang, and H. Xu, 'An efficient local Chan-Vese model for image segmentation', *Pattern Recognit.*, vol. 43, no. 3, pp. 603–618, 2010, doi: 10.1016/j.patcog.2009.08.002.

[31] Z. Ji, Y. Xia, Q. Sun, G. Cao, and Q. Chen, 'Active contours driven by local likelihood image fitting energy for image segmentation', *Inf. Sci. (Ny).*, vol. 301, no. January, pp. 285–304, 2015, doi: 10.1016/j.ins.2015.01.006.

[32] S. Yuan, P. Monkam, S. Li, H. Song, and F. Zhang, 'Active contour model via local and global intensity information for image segmentation', *Chinese Control Conf. CCC*, pp. 5618–5623, 2017, doi: 10.23919/ChiCC.2017.8028249.

[33] L. Zhao, S. Zheng, H. Wei, and L. Gui, 'Adaptive active contour model driven by global and local intensity fitting energy for image segmentation', *Optik (Stuttg).*, vol. 140, pp. 908–920, 2017, doi: 10.1016/j.ijleo.2017.05.029.

[34] Z. Wang and Y. J. Liu, 'Active contour model by combining edge and region information discrete dynamic systems', *Adv. Mech. Eng.*, vol. 9, no. 3, pp. 1–10, 2017, doi: 10.1177/1687814017692947.

[35] S. Osher and J. A. Sethian, 'Fronts propagating with curvature-dependent speed: Algorithms based on Hamilton-Jacobi formulations', *J. Comput. Phys.*, vol. 79, no. 1, pp. 12–49, 1988.

[36] V. Caselles, F. Catté, T. Coll, and F. Dibos, 'A geometric model for active contours in image processing', *Numer. Math.*, vol. 66, no. 1, pp. 1–31, 1993, doi: 10.1007/BF01385685.

[37] R. Malladi, J. A. Sethian, and B. C. Vemuri, 'Shape Modeling with Front Propagation: A Level Set Approach', *IEEE Trans. Pattern Anal. Mach. Intell.*, vol. 17, no. 2, pp. 158–175, 1995, doi: 10.1109/34.368173.

[38] G. Aubert, P. Kornprobst, and G. Aubert, *Mathematical problems in image processing: partial differential equations and the calculus of variations*, vol. 147. Springer, 2006.

[39] L. Dong, J. Lu, B. Zhao, W. Wang, and Y. Zhao, 'Review of the possible association between thyroid and breast carcinoma', *World J. Surg. Oncol.*, vol. 16, no. 1, p. 130, 2018, doi: 10.1186/s12957-018-1436-0.

[40] J. H. An *et al.*, 'A possible association between thyroid cancer and breast cancer', *Thyroid*, vol. 25, no. 12, pp. 1330–1338, 2015.

[41] Z. Huang *et al.*, 'Breast cancer incidence and mortality: trends over 40 years among women in Shanghai, China', *Ann. Oncol.*, vol. 27, no. 6, pp. 1129–1134, Jun. 2016, doi: 10.1093/ANNONC/MDW069.

[42] N. Huang *et al.*, 'Association between breast cancer and thyroid cancer: A study based on 13 978 patients with breast cancer', *Cancer Med.*, vol. 7, no. 12, pp. 6393–6400, 2018, doi: https://doi.org/10.1002/cam4.1856.

[43] R. F. Chang, W. J. Wu, C. C. Tseng, D. R. Chen, and W. K. Moon, '3-D Snake for US in Margin Evaluation for Malignant Breast Tumor Excision Using Mammotome', *IEEE Trans. Inf. Technol. Biomed.*, vol. 7, no. 3, pp. 197–201, 2003, doi: 10.1109/TITB.2003.816560.

[44] Y. L. Huang and D. R. Chen, 'Automatic contouring for breast tumors in 2-D sonography', *Annu. Int. Conf. IEEE Eng. Med. Biol. - Proc.*, vol. 7 VOLS, pp. 3225–3228, 2005, doi: 10.1109/iembs.2005.1617163.

[45] M. H. Yap, E. A. Edirisinghe, and H. E. Bez, 'Fully automatic lesion boundary detection in ultrasound breast images', *Med. Imaging 2007 Image Process.*, vol. 6512, p. 65123I, 2007, doi: 10.1117/12.708625.

[46] L. Gao, X. Liu, and W. Chen, 'Phase- and GVF-based level set segmentation of ultrasonic breast tumors', *J. Appl. Math.*, vol. 2012, 2012, doi: 10.1155/2012/810805.

[47] A. Rodtook and S. S. Makhanov, 'Multi-feature gradient vector flow snakes for adaptive segmentation of the ultrasound images of breast cancer', *J. Vis. Commun. Image Represent.*, vol. 24, no. 8, pp. 1414–1430, 2013, doi: 10.1016/j.jvcir.2013.09.009.

[48] L. Moraru, S. Moldovanu, and A. Biswas, 'Optimization of breast lesion segmentation in texture feature space approach', *Med. Eng. Phys.*, vol. 36, no. 1, pp. 129–135, 2014, doi: 10.1016/j.medengphy.2013.05.013.

[49] Y. Chang *et al.*, 'Computer-aided diagnosis for classifying benign versus malignant thyroid nodules based on ultrasound images: A comparison with radiologist-based assessments', *Med. Phys.*, vol. 43, no. 1, pp. 554–567, 2016, doi: 10.1118/1.4939060.

[50] C. M. Chen, H. H. S. Lu, and Y. C. Lin, 'An early vision-based snake model for ultrasound image segmentation', *Ultrasound Med. Biol.*, vol. 26, no. 2, pp. 273–285, 2000, doi: 10.1016/S0301-5629(99)00140-4.

[51] C. P. Loizou, C. S. Pattichis, M. Pantziaris, T. Tyllis, and A. Nicolaides, 'Snakes based segmentation of the common carotid artery intima media', *Med. Biol. Eng. Comput.*, vol. 45, no. 1, pp. 35–49, 2007, doi: 10.1007/s11517-006-0140-3.

[52] C. P. Loizou, A. Nicolaides, E. Kyriacou, N. Georghiou, M. Griffin, and C. S. Pattichis, 'A Comparison of Ultrasound Intima-Media Thickness Measurements of the Left and Right Common Carotid Artery', *IEEE J. Transl. Eng. Heal. Med.*, vol. 3, no. May, 2015, doi: 10.1109/JTEHM.2015.2450735.

[53] W. Wang, L. Zhu, J. Qin, Y. P. Chui, B. N. Li, and P. A. Heng, 'Multiscale geodesic active contours for ultrasound image segmentation using speckle reducing anisotropic diffusion', *Opt. Lasers Eng.*, vol. 54, pp. 105–116, 2014, doi: 10.1016/j.optlaseng.2013.10.003.

[54] P. Ganesh, J. J. J. Babu, and S. Suganthkannan, 'Automated Thyroid Nodule Segmentation Algorithm for Ultrasound Images', *Int. J. Adv. Res. Ectrical Electron. Instrum. Eng.*, vol. 3, no. 3, pp. 85–90, 2014.

[55] W. Du and N. Sang, 'An effective method for ultrasound thyroid nodules segmentation', *4th Int. Symp. Bioelectron. Bioinformatics, ISBB 2015*, pp. 207–210, 2015, doi: 10.1109/ISBB.2015.7344960.

[56] D. Koundal, S. Gupta, and S. Singh, 'Computer aided thyroid nodule detection system using medical ultrasound images', *Biomed. Signal Process. Control*, vol. 40, pp. 117–130, 2018, doi: 10.1016/j.bspc.2017.08.025.

[57] W. Gómez, A. F. C. Infantosi, L. Leija, and W. C. A. Pereira, 'Active contours without edges applied to breast lesions on ultrasound', *IFMBE Proc.*, vol. 29, no. 2, pp. 292–295, 2010, doi: 10.1007/978-3-642-13039-7_73.

[58] L. Cai and Y. Wang, 'A phase-based active contour model for segmentation of breast ultrasound images', *Proc. 2013 6th Int. Conf. Biomed. Eng. Informatics, BMEI 2013*, no. 2012, pp. 91–95, 2013, doi: 10.1109/BMEI.2013.6746913.

[59] R. Rodrigues, R. Braz, M. Pereira, J. Moutinho, and A. M. G. Pinheiro, 'A Two-Step Segmentation Method for Breast Ultrasound Masses Based on Multi-resolution Analysis', *Ultrasound Med. Biol.*, vol. 41, no. 6, pp. 1737–1748, 2015, doi: 10.1016/j.ultrasmedbio.2015.01.012.

[60] A. Nugroho, H. A. Nugroho, and L. Choridah, 'Active contour bilateral filter for breast lesions segmentation on ultrasound images', in *2015 International Conference on Science in Information Technology (ICSITech)*, 2015, pp. 36–40. doi: 10.1109/ICSITech.2015.7407773.

[61] L. Liu *et al.*, 'Automated breast tumor detection and segmentation with a novel computational framework of whole ultrasound images', *Med. Biol. Eng. Comput.*, vol. 56, no. 2, pp. 183–199, 2018, doi: 10.1007/s11517-017-1770-3.

[62] D. E. Maroulis, M. A. Savelonas, S. A. Karkanis, D. K. Iakovidis, and N. Dimitropoulos, 'Computer-aided thyroid nodule detection in ultrasound images', *Proc. - IEEE Symp. Comput. Med. Syst.*, pp. 271–276, 2005, doi: 10.1109/cbms.2005.44.

[63] M. Savelonas, D. Maroulis, D. Iakovidis, S. Karkanis, and N. Dimitropoulos, 'A Variable Background Active Contour model for automatic detection of thyroid nodules in ultrasound images', *Proc. - Int. Conf. Image Process. ICIP*, vol. 1, pp. 17–20, 2005, doi: 10.1109/ICIP.2005.1529676.

[64] D. E. Maroulis, M. A. Savelonas, D. K. Iakovidis, S. A. Karkanis, and N. Dimitropoulos, 'Variable background active contour model for computer-aided delineation of nodules in thyroid ultrasound images', *IEEE Trans. Inf. Technol. Biomed.*, vol. 11, no. 5, pp. 537–543, 2007, doi: 10.1109/TITB.2006.890018.

[65] M. A. Savelonas, D. K. Iakovidis, N. Dimitropoulos, and D. Maroulis, 'Computational Characterization of Thyroid Tissue in the Radon Domain', *Proc. - IEEE Symp. Comput. Med. Syst.*, pp. 189–192, 2007, doi: 10.1109/CBMS.2007.33.

[66] D. K. Iakovidis, M. A. Savelonas, S. A. Karkanis, and D. E. Maroulis, 'A genetically optimized level set approach to segmentation of thyroid ultrasound images', *Appl. Intell.*, vol. 27, no. 3, pp. 193–203, 2007, doi: 10.1007/s10489-007-0066-y.

[67] E. G. Keramidas, D. K. Iakovidis, D. Maroulis, and S. Karkanis, 'Efficient and effective ultrasound image analysis scheme for thyroid nodule detection', *Lect. Notes Comput. Sci. (including Subser. Lect. Notes Artif. Intell. Lect. Notes Bioinformatics)*, vol. 4633 LNCS, pp. 1052–1060, 2007, doi: 10.1007/978-3-540-74260-9_93.

[68] M. A. Savelonas, D. K. Iakovidis, I. Legakis, and D. Maroulis, 'Active contours guided by echogenicity and texture for delineation of thyroid nodules in ultrasound images', *IEEE Trans. Inf. Technol. Biomed.*, vol. 13, no. 4, pp. 519–527, 2009, doi: 10.1109/TITB.2008.2007192.

[69] E. A. Mylona, M. A. Savelonas, and D. Maroulis, 'Entropy-based spatially-varying adjustment of active contour parameters', *ICIP Proc.*, pp. 2565–2568, 2012.

[70] E. A. Mylona, M. A. Savelonas, D. Maroulis, and A. N. Skodras, 'Autopilot spatially-adaptive active contour parameterization for medical image segmentation', *Proc. - IEEE Symp. Comput. Med. Syst.*, pp. 268–272, 2013.

[71] E. A. Mylona, M. A. Savelonas, and D. Maroulis, 'Self-parameterized active contours based on regional edge

structure for medical image segmentation', *Springerplus*, vol. 3, no. 1, pp. 1–9, 2014, doi: 10.1186/2193-1801-3-424.

[72] Eleftheria Mylona, Michalis Savelonas, and Dimitris Maroulis, 'Automated Adjustment of Region-Based Active Contour Parameters Using Local Image Geometry', *IEEE Trans. Cybern.*, vol. 44, no. 12, pp. 2757–2770, 2014, [Online]. Available: http://ieeexplore.ieee.org/xpl/articleDetails.jsp?tp=&arnumber=6803910&queryText%3Dsavelonas

[73] H. A. Nugroho, A. Nugroho, and L. Choridah, 'Thyroid nodule segmentation using active contour bilateral filtering on ultrasound images', in *2015 International Conference on Quality in Research (QiR)*, Aug. 2015, pp. 43–46. doi: 10.1109/QiR.2015.7374892.

[74] H. A. Nugroho, Zulfanahri, A. Nugroho, E. L. Frannita, I. Ardiyanto, and L. Choridah, 'Feature extraction based on laws' texture energy for lesion echogenicity classification of thyroid ultrasound images', in *2017 International Conference on Computer, Control, Informatics and its Applications (IC3INA)*, 2017, pp. 41–46. doi: 10.1109/IC3INA.2017.8251737.

[75] H. A. Nugroho, E. L. Frannita, A. Nugroho, Zulfanahri, I. Ardiyanto, and L. Choridah, 'Classification of thyroid nodules based on analysis of margin characteristic', *Proc. - 2017 Int. Conf. Comput. Control. Informatics its Appl. Emerg. Trends Comput. Sci. Eng. IC3INA 2017*, vol. 2018-Janua, pp. 47–51, 2017, doi: 10.1109/IC3INA.2017.8251738.

[76] P. Poudel, C. Hansen, J. Sprung, and M. Friebe, '3D segmentation of thyroid ultrasound images using active contours', *Curr. Dir. Biomed. Eng.*, vol. 2, no. 1, pp. 467–470, 2016, doi: 10.1515/cdbme-2016-0103.

[77] J. Xu, K. Chen, X. Yang, D. Wu, and S. Zhu, 'Adaptive level set method for segmentation of liver tumors in minimally invasive surgery using ultrasound images', *2007 1st Int. Conf. Bioinforma. Biomed. Eng. ICBBE*, pp. 1091–1094, 2007, doi: 10.1109/ICBBE.2007.282.

[78] A. Sarti, C. Corsi, E. Mazzini, and C. Lamberti, 'Maximum likelihood segmentation of ultrasound images with rayleigh distribution', *IEEE Trans. Ultrason. Ferroelectr. Freq. Control*, vol. 52, no. 6, pp. 947–960, 2005, doi: 10.1109/TUFFC.2005.1504017.

[79] T. F. Chan and L. A. Vese, 'Active contours without edges', *IEEE Trans. Image Process.*, vol. 10, no. 2, pp. 266–277, 2001, doi: 10.1109/83.902291.

[80] A. Nugroho, R. Hidayat, H. A. Nugroho, and J. Debayle, 'Ultrasound object detection using morphological region-based active contour: An application system', *Int. J. Innov. Learn.*, vol. 29, no. 4, pp. 412–430, 2021, doi: 10.1504/IJIL.2021.115497.

[81] A. Nugroho, 'SIMPLIFIKASI MODEL CV BERPADU OPERASI MORFOLOGI UNTUK DETEKSI OBJEK KANKER PADA CITRA USG', *J. Inform. Polinema*, vol. 8, no. 2, pp. 49–56, 2022, doi: 10.33795/jip.v8i2.923.

[82] A. Nugroho, A. Fauzi, B. Sunarko, H. Wibawanto, A. Mulwinda, and N. Iksan, 'Web based application system for cancerous object detection in ultrasound images', *AIP Conf. Proc.*, vol. 2727, no. 1, 2023, doi: 10.1063/5.0141519.

[83] A. Nugroho, R. Hidayat, H. A. Nugroho, and J. Debayle, 'Development of Active Contour Model For Radiological Ultrasound Image Segmentation', Universitas Gadjah Mada, 2021.

[84] S. Ruuska, W. Hämäläinen, S. Kajava, M. Mughal, P. Matilainen, and J. Mononen, 'Evaluation of the confusion matrix method in the validation of an automated system for measuring feeding behaviour of cattle', *Behav. Processes*, vol. 148, pp. 56–62, 2018.